Journal of Fluids and Structures (2000) **14,** 735–751
doi:10.1006/jfls.2000.0291, available online at http://www.idealibrary.com on IDEAL®

VIBRATION OF CAVITATING ELASTIC WING IN A PERIODICALLY PERTURBED FLOW: EXCITATION OF SUBHARMONICS

E. AMROMIN

Mayo Foundation, 52131 street NW, Rochester, MN 55905, U.S.A.

AND

S. KOVINSKAYA

Mechmath LLC, Rochester, MN 55901, U.S.A.

(Received 17 June 1998, and in final form 3 February 2000)

The vibration of an elastic wing with an attached cavity in periodically perturbed flows is analyzed. Because the cavity thickness and length L also are perturbed, an excitation with a fixed frequency ω leads to a parametric vibration of the wing, and the amplitudes and spectra of its vibration have nonlinear dependencies on the amplitude of the perturbation. Numerical analysis was carried out for a two-dimensional flow of ideal fluid. Wing vibration was described by means of the beam equation. As a result, two frequency bands of a significant vibration increase were found. A high-frequency band is associated mainly with an elastic resonance of the wing, and a cavity can add a certain damping. A low-frequency band is associated with cavity-volume oscillations. The governing parameter for the low-frequency vibration is the cavity length-based Strouhal number $\mathrm{St}_C = \omega L/U$, where U is the free-stream speed. The most significant vibration in the low-frequency band corresponds to approximately constant values of Sh_C and has the most extensive subharmonics.

1. INTRODUCTION

CONSIDERATION OF THE HYDROELASTIC problem for a cavitating wing is provoked by a difficulty in the practice of model ship basins. Figure 1 is plotted on the basis of measurements of sound pressure levels for a cavitating marine propeller and its model by Blake (1986); an example of this difficulty is thereby provided. Results of a model test extrapolation for full-scale condition by conventional formulas are shown. A discrepancy in this extrapolation for the cavitating marine propeller with full-scale experimental data has several peaks in the low-frequency band. This discrepancy is particularly significant in a high-frequency band that contains frequencies of the first elastic resonance of blades of the full-scale marine propeller. A similar problem occurs with pumps. Therefore, it is necessary to analyze unsteady hydroelastic effects in the cavitating flow around the blades and their responses to customary periodic excitations. An excitation of the cavitating blade is caused mainly by a periodic variation of the incoming flow. This variation is associated with the blade rotation in a nonuniform velocity field (for example, in the wake of a ship hull). A boundary layer pulsation also can contribute to this excitation.

A reasonable initial step in a mathematical investigation of the cause of the above discrepancy would consist of computations of an amplitude response of the blades to

0889–9746/00/070735 + 17 $35.00/0

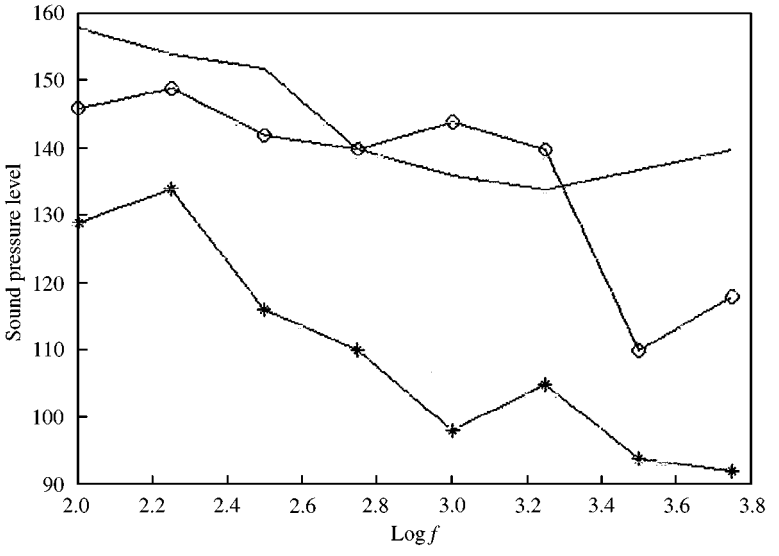

Figure 1. Typical variations of a cavitating marine propeller pressure sound level with the frequency f(Hz): —∗—, model test results; —◇—, full-scale data; ——, conventional extrapolation of this model test for full-scale conditions.

mono-frequency excitations in the large band of frequencies. The fundamentals for such an analysis, however, are not ready. The contemporary theoretical methods of cavitation analysis are well developed for two-dimensional steady flows (Rowe & Blottiaux 1993; Amromin & Vaciliev 1994; Dang & Kuiper 1998). Nevertheless, even the recent investigations of unsteady cavitating flows by Boulon & Chahine (1998) and Shin & Ikohagi (1998) are far from an analysis of certain general characteristics of these unsteady phenomena (including an analysis of hydrofoil amplitude responses). The elastic cavitating wings were analyzed earlier in steady flow only, by Rashad & Green (1990).

It is appropriate to emphasize that the hydroelastic problem for cavitating hydrofoils/wings basically is different from the hydroelastic problems in aviation, because three media are interacting in the cavitating flows, and an oscillating boundary between gas and fluid introduces multi-frequency perturbations as a response to any excitation of the incoming flow, including the one-frequency excitation. Thus, the well-developed hydroelastic theory of noncavitating wings cannot be a sufficient basis for this examination. The first step in the examination of the effects of cavitation on the hydrofoil/blade vibration can be done with several relatively simple assumptions that are not fully satisfactory. Particularly, it concerns the Joukovski–Kutta condition. This condition is not good for both high values of reduced frequencies (Archibald 1975) and large partial cavities (Amromin & Vaciliev 1994). Such assumptions influence numerical results, but do not prevent qualitative comparisons and finding the most significant aspects of an interaction of cavities with the elastic wings.

The authors of this paper analyzed the two-dimensional cavitating flows near elastic wings; their goal in analyzing of hydroelastic effects on cavitating unsteady flows was to estimate the roles of different physical factors. Their most significant results were obtained for a low-frequency band of the flow excitation; the physical base of a nonlinear amplification of vibrations by cavities was clarified. They found that this amplification is associated with a rise of the subharmonics for several significant frequencies.

2. MATHEMATICAL FORMULATION

An unsteady two-dimensional hydroelastic problem for the cavitating wing is considered here. Let E, I, ρ, $\delta(x)$ represent Young's modulus, the inertia moment, the density, and the thickness of a wing, respectively. Let this thickness be small relative to the wing chord. The wing vibration is described as a beam vibration in the bending motion. A time-dependent wing camber line displacement V then can be determined by the following equation of the flexural beam vibration:

$$\frac{\partial^2}{\partial x^2}\left(EI\frac{\partial^2 V}{\partial x^2}\right)+\rho\delta\frac{\partial^2 V}{\partial t^2}=F, \tag{1}$$

where F is a hydrodynamic force that acts along the perpendicular to the wing chord. Because of the consideration of ideal incompressible fluid, a velocity potential Φ can be introduced here, and F can be found from the integral of the fluid momentum equations (the Euler equations). If S is the wing surface, N is normal to S (see Figure 2), and V_N is the velocity of the wing surface normal motion, then Φ is the solution of the following boundary-value problem for the Laplace equation:

$$\Delta\Phi=0; \qquad \frac{\partial\Phi}{\partial N}\,|_S=V_N, \qquad \{\text{grad}\,\Phi\}_{x\to-\infty}=\{\cos\alpha,\sin\alpha\}, \tag{2)–(4}$$

where α is the angle of attack of the wing. An additional condition must be applied at the trailing edge of the wing (at $x=C$); usually, it is the Jukovski–Kutta condition. Because the pressure within cavities is constant, the existence of a cavity over the wing makes it necessary to add a boundary condition on the corresponding part of S. The substitution of

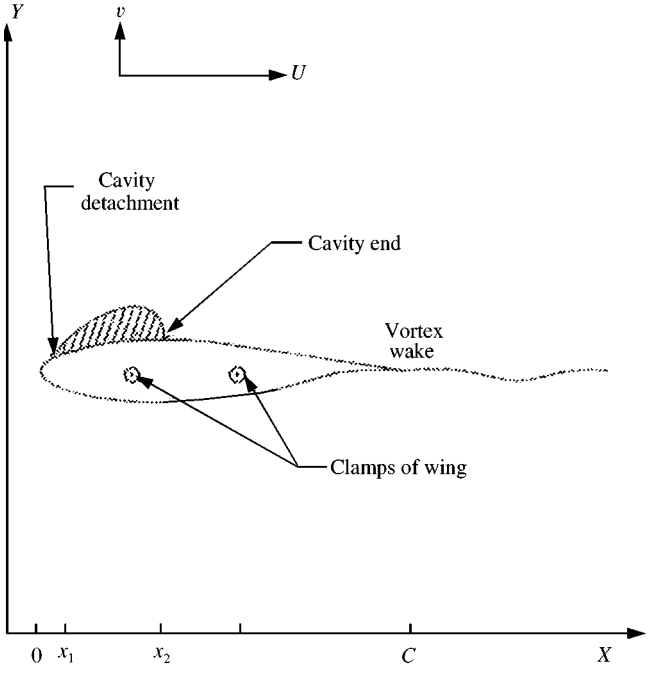

Figure 2. Sketch of the cavitating wing and of the flow structure.

the pressure constancy condition into the momentum equation results in the following equation:

$$\frac{\partial \Phi}{\partial t} + |\operatorname{grad} \Phi|^2_{S_c} = 1 + \sigma, \tag{5}$$

where $\sigma = 2(P_{00} - P_c)/\rho^* U^2$ is the cavitation number, ρ^* is the density of the fluid, P_c is the pressure within the cavity, P_∞ and U are the pressure and the free-stream speed of the unperturbed flow upstream of the wing, and S_C is the cavity surface. This surface must be found for any given σ using a selected cavity scheme. Generally, problem (2)–(5) with a selected condition for the velocity at the trailing edge is a nonlinear unsteady problem. Such a problem is still too difficult for a detailed numerical simulation without further simplification. For this reason, the unsteady cavitating flow is considered to be a perturbed steady cavitating flow and the following velocity potential is used:

$$\Phi(x, y, t) = \Phi_0(x, y) + \Phi_1(x, y)\, e^{i\omega t} + \Phi_2(x, y, \Gamma) + \Phi_3(x, y, Q), \tag{6}$$

where the potential Φ_0 defines the time-average flow, the potential Φ_1 gives the incoming flow perturbation, the potential Φ_2 is associated with the intensity $\Gamma(x, t)$ of the vortices (these vortices are distributed along the chord and downstream from the wing), and Φ_3 is the potential of the sources. These sources are distributed along a part of the chord and have a density of $Q(x, t)$; thus, Φ_3 is defined by the following formula:

$$\Phi_3(x, y, t) = \frac{1}{\pi} \int_{S_c} Q(x, t) \ln |(x - \zeta)^2 + y^2| \, d\zeta.$$

Because the combination of the potentials Φ_2 and Φ_3 is adequate for modeling of any small-amplitude unsteady response and this combination allows the estimation of the effect of the unsteady vortex wake on the flow, it is possible to avoid the use of a quasi-steady approach here.

The employment of the potential (6) generally can lead to an infinite increase in the left-hand side of equation (5) because of an increase of $\partial\Phi/\partial t$. This logarithmic infinity can appear at $|x| \to \infty$ (or at $|y| \to \infty$) if the total density of the sources does not equal zero. The introduction of a fictitious free surface far over the wing (at $y = Y \gg C$) removes this mathematical difficulty from the 2-D analysis of the unsteady cavities.

Assume that the potential Φ_0 is known (as well as the time-average cavity length L), the flow perturbation is relatively small, and the cavity is thin. The wing displacement V, the intensity of the vortices Γ and the density of the sources Q are then small, and condition (3) can be linearized relative to the above-mentioned small quantities; then this condition can be considered along the wing chord. It follows, then, that the cavity pulsation can be analyzed as a small oscillation of the impermeable boundary of the potential flow, all derivations of the velocity potential can be approximated by linear functions, and the following equation can be used for the density $Q(x, t)$:

$$Q(x, t) = \frac{\partial [H(x, t)\, \partial\Phi/\partial x(x, t)]}{\partial x} + \frac{\partial H(x, t)}{\partial t}, \tag{7}$$

where Q is presented as a function of the cavity thickness H [see a similar formula in Dowell *et al.* (1995); actually, H is the distance between the cavity and the wing surface]. Consequently, this density depends linearly on the oscillations of the cavity thickness. The cavity length also oscillates. Keeping this in mind, equation (7) has to be considered in points with the time-dependent abscissa x, which is quite complex. Of course, it would be preferable to distribute sources along a fixed segment. It is possible to do such a fixing with the use of

series relative to degrees of L/C, where L is the time-averaged cavity length. An analysis of this approach with consideration of the first degree of L/C is done in this paper, and the time-dependent cavity length is presented as $L_t(t) \equiv l(t) + L < C$. It is important to note that the cavity length oscillation modulus $|l(t)|$ is not necessarily small relative to L (see several known experimental data presented in Figure 3).

Let the instantaneous abscissa of a point on the cavity be $x + \xi l(t)$, where the values of x and of the ratio $\xi = (x - X_1)/L$ do not depend on t (X_1 and X_2 are time-averaged abscissas of the streamline detachment and reattac behind the cavity). Then the following linear extrapolation of the time-independent function at the time-dependent point can be introduced:

$$U_0(x + \xi l) \approx U_0(x) + \frac{\mathrm{d}U_0}{\mathrm{d}x}\,\frac{l(t)}{L}\,(x - X_1), \tag{8}$$

where $U_0 = \partial\Phi_0/\partial x$ is the unperturbed velocity. In such a relationship, the velocity U is a function of l and the time-averaged abscissa x, but the oscillations of the normal component of the velocity are associated with the oscillations of H and the camber-line oscillations. The substitution of equation (8) into equation (7) leads to the appearance of the product of the time-dependent functions in the formulas for $Q(x, t)$ and, consequently, in the potential Φ_3. This circumstance leads to an appearance of a multi-frequency response of the cavitating wing on the mono-frequency excitation. Therefore, all unknown functions must be defined as series. Thus,

$$V(x, t) = \sum_{k=1}^{M} V_K\, \mathrm{e}^{\mathrm{i}\omega kt}, \tag{9}$$

where $V_K = v_{1,k}(x) + \mathrm{i}v_{2,k}(x)$, and similar series have to be written for Q, H and Γ. Moreover, the cavity length oscillation $l(t)$ must be defined by the series

$$l(t) = \sum_{k=1}^{M} [l_{1,k} + il_{2,k}]\, \mathrm{e}^{\mathrm{i}\omega kt}. \tag{10}$$

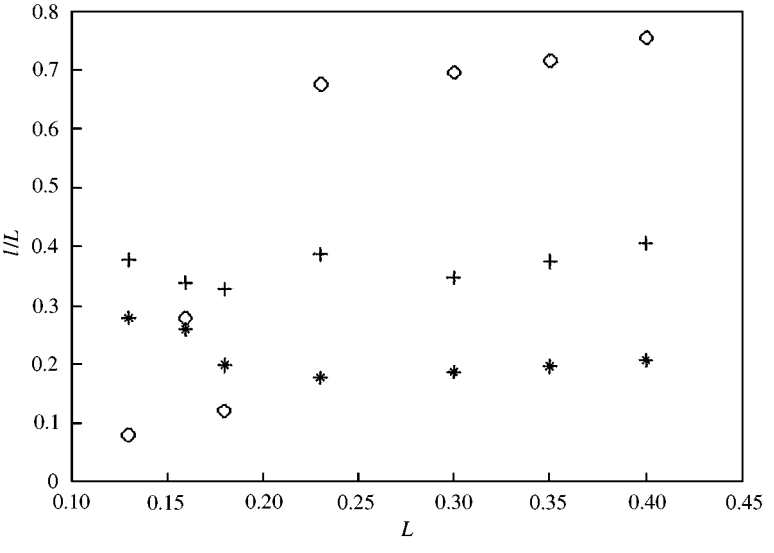

Figure 3. The relative cavity-length oscillation magnitudes. Experimental data: ◇, Amromin *et al.* (1994) for NACA-16009 hydrofoil; ∗, by Yamaguchi & Kato (1983) for EN hydrofoil; +, by Pellone and Rowe(1988) for NACA-0010.

Substitution of equation (10) into equations (7, 8) gives

$$Q_K(x) = \mathrm{i}\,JH_K(x) + \frac{\partial[H_K(x)\,U_0(x)]}{\partial x} + \frac{\partial U_0}{\partial x}(x)\sum_{S=1}^{K} H_s(x)\,[l_{1,k-S} + \mathrm{i}\,l_{2,k-S}], \qquad (11)$$

where $J = k$ St is the Strouhal number based on the chord length $C(\mathrm{St} = \omega C/U)$. In this result, the right-hand side of equation (11) contains a product of the coefficients of the above series even for small flow perturbations.

Because the infinite vortex wake runs along a radius downstream from the trailing edge of the wing, the solution to the problem (2)–(4) can be found using a succession of the Birnbaum equations. The original Birnbaum equation was deduced for periodically perturbed flows from equations (2) and (3), while taking into account the Joukovski–Kutta condition in the form $\Gamma_K(1) = 0$ and the Helmholtz theorem for the vortex sheet. Such an equation is convenient for computation; it reduces the unsteady problem for the infinite interval to a steady problem for the segment. For successive k indices, the following succession of the equations is deduced:

$$\delta_K^1 \frac{\partial \Phi_1}{\partial y} = \mathrm{i}\,J(V_K + H_K/2) - \frac{1}{\pi}\int_0^1 \frac{\Gamma_K}{x-\xi}\,\mathrm{d}\xi - \frac{\mathrm{i}J}{\pi}\int_0^1 \Gamma_K\,\mathrm{e}^{\mathrm{i}J(x-z)}\int_{J(z-x)}^{\infty}\frac{\mathrm{e}^{\mathrm{i}w}}{w}\,\mathrm{d}w\,\mathrm{d}z, \qquad (12)$$

where the symbol δ_K^1 is equal to 1 for $k = 1$, but in other cases $\delta_K^1 = 0$. The chord length C is taken as the unit of length in equation (12) and in what follows. For the well-known case of the rigid noncavitating wing, $M = 1$ in equation (10) and $H_K = V_K = 0$ in equation (12). If the hydrofoil is the flat plate (having a zero thickness) and $H_K = 0$ (without any cavity), then equation (12) corresponds to the Theodorsen problem; thus, a match with the known hydroelastic results is presented here.

The displacement $V(x, t)$ for elastic wings must be determined from equation (1). According to the above assumptions, equation (1) was reduced to the following succession of equations:

$$\frac{\partial^2}{\partial x^2} EI \frac{\partial^2 V_K}{\partial x^2} - \rho\delta V_K J^2 = \rho^*(\Gamma_K U_0 + \mathrm{i}J\int_0^x \Gamma_K\,\mathrm{d}z). \qquad (13)$$

Here the complex modulus of elasticity $E = E_1(1 + \mathrm{i}\eta)$ depends on Young's modulus E_1 for the wing material and the dissipation coefficient η. The first term on the right-hand side of equation (13) describes the Joukovski force contribution to the hydrodynamic loads on the wing, while the second term is associated with the added mass of the water. The following conditions correspond to the rigid wing clamping in the points with the abscissas $x = CX_a$ and $x = CX_c$:

$$V_K(X_a) = V_K(X_c) = \frac{\partial V_K}{\partial x}(X_a) = \frac{\partial V_K}{\partial x}(X_c) = 0. \qquad (14)$$

This type of clamping is common for tunnel tests [see Franc *et al.* (1995), for example]. The wing edges are free, so the edge forces and moments vanish:

$$\frac{\partial^2 V_K}{\partial x^2}(0) = \frac{\partial^3 V_K}{\partial x^3}(0) = \frac{\partial^2 V_K}{\partial x^2}(1) = \frac{\partial^3 V_K}{\partial x^3}(1) = 0. \qquad (15)$$

Equation (5) has to be considered only along the cavity, where $U_0 = \sqrt{1+\sigma}$ in the time-averaged flow. Taking into account equation (11) and using linearizations for equation (5) in the whole, it is possible to use the cavity length oscillation as a small parameter. This

equation then can be transformed into succession of the following set of equations:

$$2J\delta_K^1 \frac{\partial \Phi_1}{\partial x} + U_0 \frac{\partial \Gamma_K}{\partial x} + (\partial\sigma/\partial L)\,[l_{1,k} + \mathrm{i}l_{2,k}] + \mathrm{i}J\Gamma_K = \frac{1}{\pi}\int_x^{X_1}\left[\frac{U_0 Q_K}{X_1 - z} - \mathrm{i}JQ_K\right]\frac{\mathrm{d}z}{x - z}. \quad (16)$$

The coefficients of equation (16) contain quantities which are the result of computations of the time-averaged cavitating flow around the same wing: these quantities are U_0 and $\sigma(L)$. U_0 is the result of a computation for the fixed σ, but the functions $\sigma(L)$ can be obtained only from a succession of such computations. This function relates to the general cavitation performance of the wing in steady flow. Examples of these computations for the 2-D wing NACA-16009 within a narrow tunnel are presented in Figure 4; the numerical results by Amromin & Vaciliev (1994) and by Rowe & Blottiaux (1993) are very close to the experimental data.

Finally, one needs to find the cavity length oscillation $l(t)$. The necessary equation appears from the geometric condition: it is clear from equation (7) that the linear dependence of Q on the limited cavity thickness H demands that only the limited values of Q be used. The singular integral equation (16), however, can have a limited solution $Q_k(x)$ only when the following additional condition is satisfied (Gakhov 1966):

$$\int_{X_1}^{X_2} \frac{G(x)}{\sqrt{(X_2 - x)(x - X_1)}}\,\mathrm{d}x = 0, \quad (17)$$

where $G(x)$ is the left-hand side of equation (16). It is possible to determine the oscillation of the cavity length l_k from equation (17) for all values of k. Thus, equations (7), (12), (13) and (16) with conditions (14), (15) and (17) make it possible to determine the four functions V, Q, H, Γ and the value of l for any value of t. The more detailed forms of these equations (with the separation of their real and imaginary parts) were written recently by Kovinskaya and Amromin (1998).

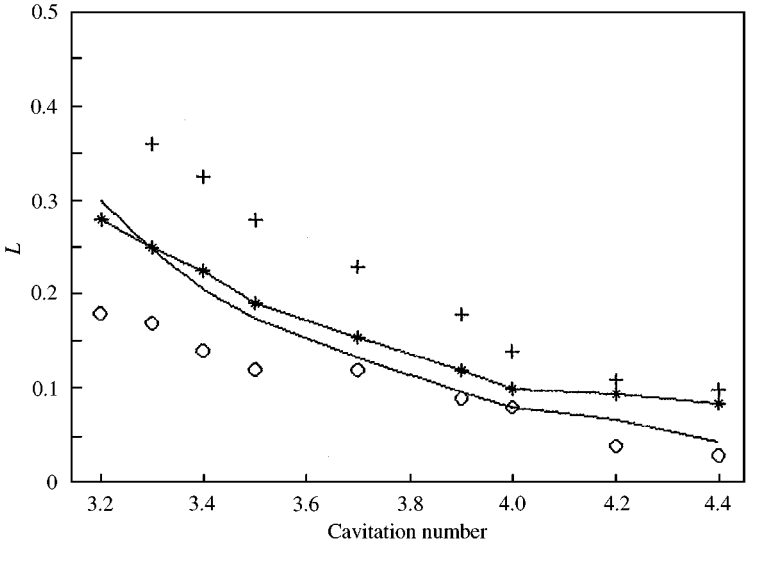

Figure 4. Computations of measured cavity length and computed time-averaged cavity length over NACA-0010 hydrofoil. ∗, Rowe & Blottiaux (1993) method; ——, Amromin & Vaciliev (1994) method; ◇, minimum of the measured length; +, maximum of the measured length.

Keep in mind that computation of the oscillations of the hydrodynamic quantities in cavitating flows is the main goal of this analysis. These oscillations are associated with cavity volume and body (blade) lift. Thus, the oscillations of the wing lift and the cavity volume are the principal results here. The series for the lift coefficient and the cavity volume oscillations are introduced as

$$C_l = \sum_{m=1}^{M} |C_{lm}| e^{i\omega mt}, \quad w = \sum_{m=1}^{M} |W_m| e^{i\omega mt}.$$

The customary way to estimate periodic perturbations is to consider a gust flow. Then the velocity perturbation potential has to be used in the form $\Phi_1 = uy$, where u is a small constant. The following dimensionless characteristics are introduced for the analysis of the numerical results:

$$V_{\text{lead}} = \frac{1}{C}\int_0^{C/2} V\,dx, \quad V_{\text{trav}} = \frac{1}{C}\int_{C/2}^{1} V\,dx, \quad C_y = C_l U/u, \quad W = wU/uC^2. \qquad (18)$$

Two different definitions of the camber-line displacement result from the intention to show the cavity influence on this displacement; this influence is associated with pressure redistribution under the cavity. It is necessary to stress at this point the use of the terminology: "lift oscillation" and "cavity volume oscillation" relates to the two last dimensionless parameters only.

The just-described mathematical model of the cavitating wing vibration operates with eight dimensionless parameters. These parameters are the cavitation number σ, the Strouhal number St, the ratio $R_1 = \rho^*/\rho$ of fluid and wing material densities, the parameter $\mu = E_1/(\rho U^2)$ that is the square of the ratio of the sound velocity in the wing material to the free-stream speed (this parameter is analogous to the square of a Mach number), the relative amplitude of a gust flow u, the coefficient of loss η for the wing material (for metals this coefficient usually varies from 0·05 up to 0·2), and two parameters related to cavitation (the cavity length and the cavity detachment point). The abscissas of the clamping points also could be considered as parameters of this mathematical problem.

3. VIBRATION OF NONCAVITATING WINGS

In looking for the cavitation effects on wing vibration in a gust flow, it is necessary to carry out a preliminary analysis for noncavitating wings. The dimensionless lift and deformations (18) are studied as functions of the Strouhal number. A typical example of such functions is presented in Figure 5. It shows an amplitude response of the lift oscillation. The basic examples for both noncavitating and cavitating flows are examined in this paper for $\mu = 0{\cdot}006$, $R_1 = 0{\cdot}36$ (this value corresponds to the water–aluminum pair), and $\eta = 0{\cdot}05$. This triad of values is usually used in the computations presented, and only a parameter from this triad can be varied in these computations. Thus, the amplitude responses of the lift oscillation and the edge vibrations for the rather speculative mercury–aluminum pair ($R_1 = 4{\cdot}95$) in Figure 6 are obtained for the same values of μ and η. Figures 5 and 6 are plotted by varying the St values with a step of 1; a logarithmic scale is conventional for such an analysis.

For the same water–aluminum pair, the band of frequencies around elastic resonance near St = 200 is presented in Figure 7 in more detail. This comparison of the vibration levels for different values of losses ($\eta = 0{\cdot}05$ and $0{\cdot}2$) helps in understanding the technique of identification of the elastic resonance frequency between numerous frequencies of high-level oscillations. The losses have a significant influence on the vibration level, only at the elastic

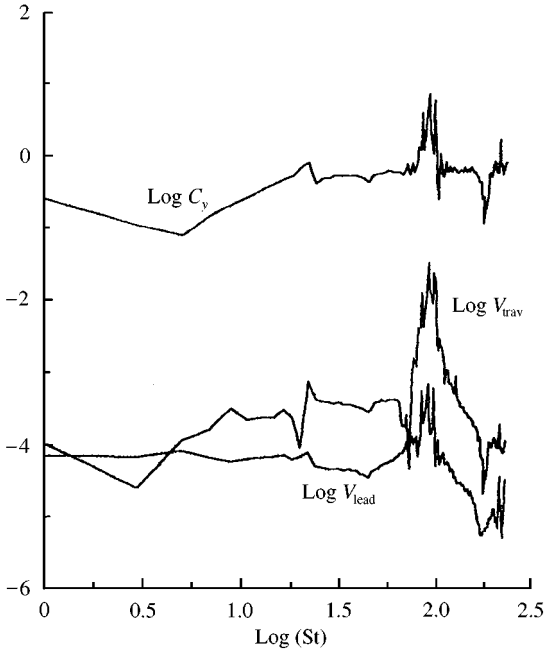

Figure 5. Strouhal number effect on the vibration of the noncavitating wing in the water. The amplitudes of displacement of the leading and trailing edges are related to the wing chord.

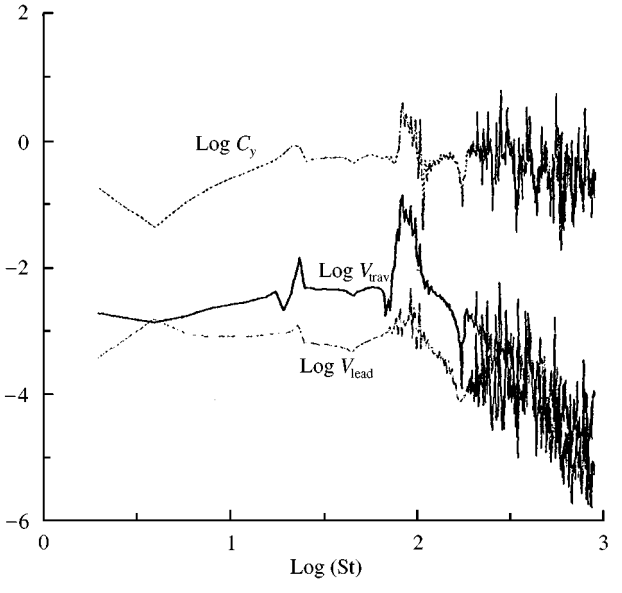

Figure 6. Strouhal number effect on the vibration of the noncavitating aluminium wing in mercury.

resonance frequency, because the displacement oscillation amplitudes are inversely proportion to the loss coefficient only near a resonance. Therefore, a loss variation is a sure way to identify the resonance of the cavitating wings, as it was also shown earlier by Kovinskaya & Amromin (1997). Observation of the curves in these figures lets us note that all functions

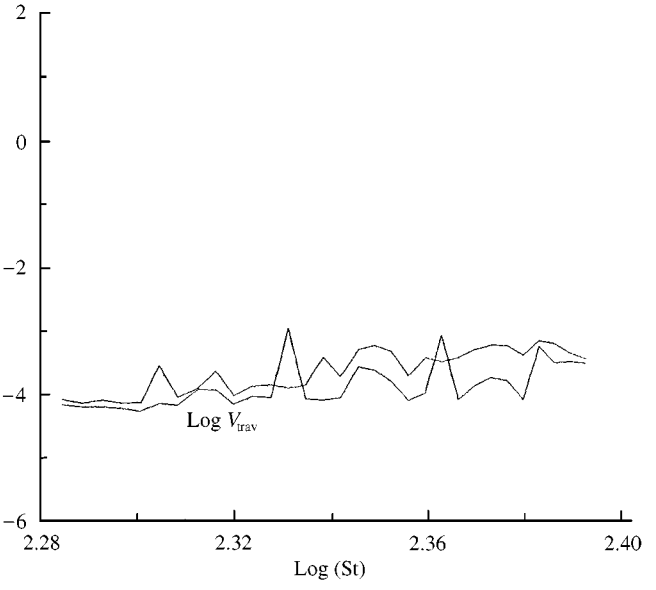

Figure 7. The loss effect on the trailing edge displacement near the elastic resonance of wing. The wing material is steel 316SS (thus, $\mu = 0{\cdot}001$ in the actual incoming flow). The curve with the higher pea corresponds to $\eta = 0{\cdot}05$; that with the lower peaks corresponds to $\eta = 0{\cdot}2$.

C_y(St) are similar, and the values of R_1 and μ do not have a qualitative influence on C_y(St), although the displacement amplitudes depend on these ratios considerably.

The studied interval of St values can be divided into two parts. Vibration in the high-frequency part of this interval is governed principally by elastic forces and has a certain quantitative dependence on μ. The elastic resonance frequencies also depend on this parameter. In the low-frequency band the elastic forces are relatively not high. The lift increases are associated with the hydrodynamic interaction. The unsteady vortex sheet downstream from the trailing edge introduces the second linear scale in this problem: it is U/ω, and the Strouhal number is just the ratio of C to this scale. In the low-frequency band, the vibration increases near certain singular values of St as a result of the interaction of hydrodynamic damping and the added mass reaction. Within this band, the frequencies of the high-level vibration do not depend on either the values of $\{R_1, \mu\}$ or on the wing shape.

4. ANALYSIS OF CAVITY INFLUENCE

The main cavitation impact on the wings is associated with changes in their lift. Therefore, it is reasonable to start the examination of cavitation of the elastic wings by analyzing their lift amplitude responses. An example of the elastic cavitating wing lift amplitude response is given in Figure 8. The excitation of subharmonics for one-frequency excitation is illustrated there; the figure presents the three first harmonics. Each of these harmonics has two significant maxima within the band $0{\cdot}5 < \log \mathrm{St} < 1{\cdot}5$; for the harmonic number k, the highest response takes place at the first (low-frequency) maximum (for $\mathrm{St} = \mathrm{St}_k$), and the products $k\mathrm{St}_k$ are close to a constant.

The comparison of the responses of the same wing in cavitating and cavitation-free flows is given in Figure 9. The response of the cavitating wing is computed, while taking into account the contribution of all harmonics. This comparison shows two frequency bands

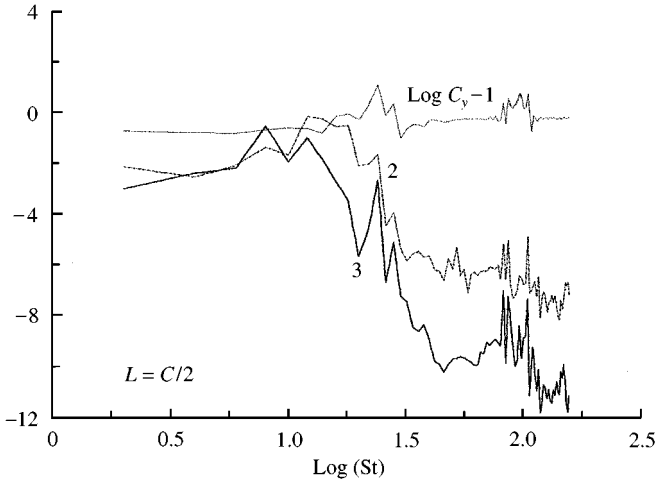

Figure 8. Comparison of the lift oscillation harmonics for the cavitating hydrofoil. The numbers near the curves mark the harmonic numbers.

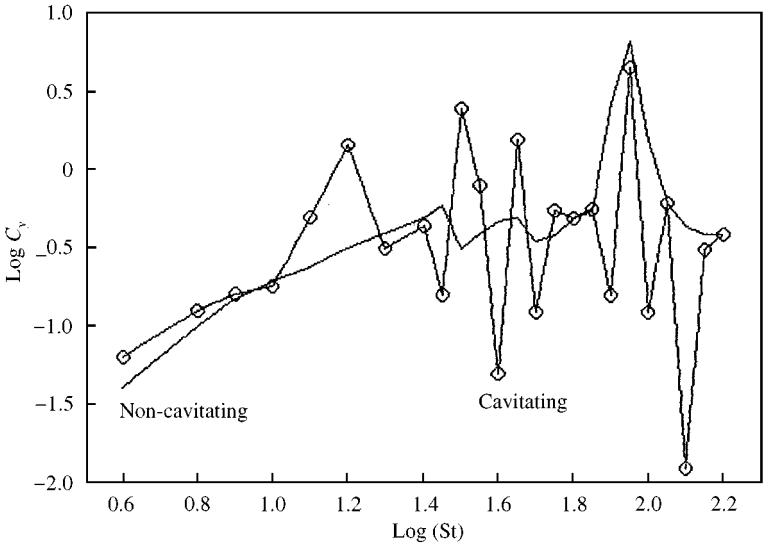

Figure 9. Comparison of the dimensionless lift oscillation for the noncavitating and cavitating wings.

where the cavity significantly influences the lift amplitude response. The ratio of the unsteady vortex sheet typical scale U/ω to the time-averaged cavity length L has diverse orders in the diverse frequency bands. In the band of the low-frequency rise of vibration, the above scale and L are comparable; consequently, depending on the value of the ratio $[(2\pi U/\omega)/4]/L$, the cavity–vortex sheet interaction can reduce or amplify the wing vibration. In the high-frequency band, this ratio is too small, and the cavity filters perturbations as a large free boundary of the non-heavy fluid. Obviously, therefore, the cavity does not add a remarkable contribution to the high-frequency vibration. The distinct points of an essential reduction of the wing amplitude response near frequencies of the elastic resonance can be explained by the above filtration of perturbations by the cavities; the cavity-free

surface of the wing cannot make such a filtration at the same frequency. It is necessary to add that large cavities can cause a small change in the elastic resonance frequencies; such a change does not exceed 2%.

The joint consideration of the lift and cavity volume oscillations clarifies the low-frequency rise of the wing response and Figure 10 is useful for this consideration. It shows amplitudes of the multi-frequency lift oscillation and the cavity volume oscillations. There is an evident correlation of the two plotted curves in the low-frequency band ($1{\cdot}15 < \log \mathrm{St} < 1{\cdot}5$; the band of such a correlation will be different for another cavity length). The additional lift oscillation peaks in Figures 9 and 10 are associated with the influence of the cavity volume oscillations.

Typical sets of cavity volume harmonics (for $k = 1, 2, \ldots, 7$) are presented in Figure 11. These sets can be different principally at the different values of the Strouhal number, even for a cavity of fixed length. The most significant cavity oscillations take place at the almost

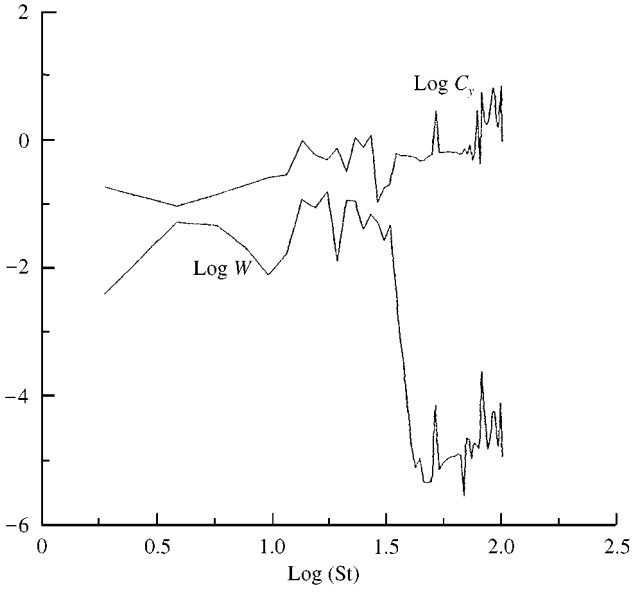

Figure 10. The lift and cavity volume oscillations versus log St.

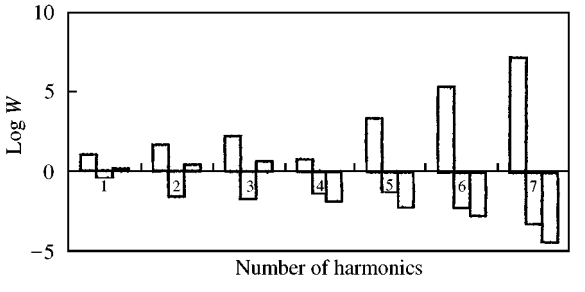

Figure 11. Typical harmonics of the cavity volume oscillation. The computations are carried out for $u = 0{\cdot}01$ and $L/C = 0{\cdot}5$. The first column in each triad of harmonics corresponds to the unstable cavity that exists at $\mathrm{St} = 2{\cdot}81$; the second one corresponds to the cavity with the about linear response on the excitation ($\mathrm{St} = 4{\cdot}71$); the third one corresponds to the cavity with the significantly nonlinear response on excitations ($\mathrm{St} = 13{\cdot}27$)

constant values of the modified Strouhal number $St_c = L\omega/U$ based on the cavity length L. This modified Strouhal number is more acceptable to the identification of the most significant frequencies. The numerical analysis allows determination of this modified Strouhal number. The dependency of this number on the time–averaged cavity length is given in Figure 12. Recent experimental data (Kawanami *et al*., 1998) gives an approximate constant St_c.

Of course, the dependencies of subharmonics on the perturbation amplitude are nonlinear and the relative contributions of harmonics depend on this amplitude, as well as the response as a whole. This affirmation is proven in Figure 13. The time-averaged cavity length, however, has a more essential influence on the wing responses.

5. SCALE EFFECTS OF SUBHARMONICS

It is appropriate at this point to clarify the role of subharmonics in the scale effects of unsteady cavitation. Returning to the initial inquiry about extrapolations of model test results, it is necessary to point out all essential discrepancies in model and full-scale conditions for marine propellers.

The model tests are carried out at the same values of the Strouhal number, but even fixing the cavitation number is practically impossible for propellers. The first discrepancy appears because the ratio $(P_{00} - P_c)/\rho^* U^2$ can be varied from $-rg/U^2$ to rg/U^2, where r is the radius of the blade and g is the gravitational acceleration. Such a variation is very small relative to an average value of σ for a propeller model of a small radius in water tunnels, but this variation must be taken into account under full-scale conditions.

The second discrepancy is associated with the Reynolds number Re effect on the incoming flow. Model tests for marine propellers are often carried out past the models of the corresponding ship hulls; thus, the model incoming flow becomes nonuniform. A certain difference in the velocity profile is caused by the Re effect, as is clear from experimental data. Therefore, the excitation spectrum is different in two compared cases, and the corresponding difference in the perturbation amplitudes should not be neglected.

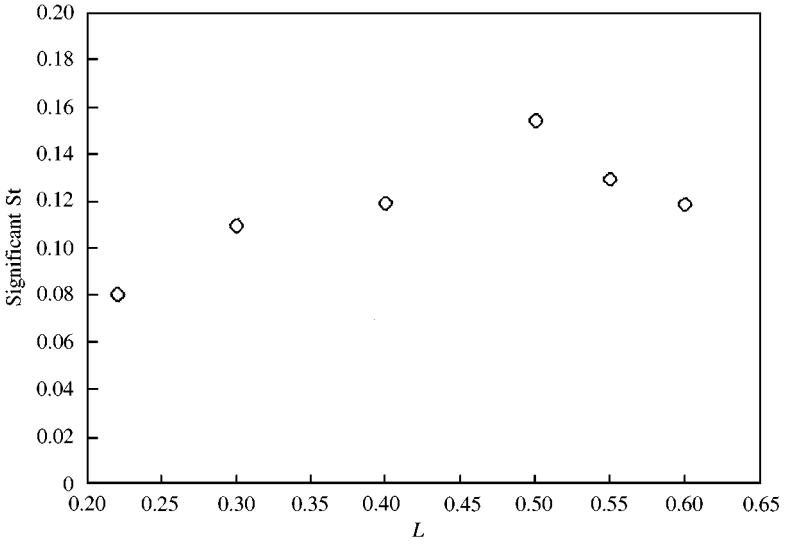

Figure 12. Cavity length-based Strouhal number for the most significant of the cavity oscillations as a function of the cavity of length.

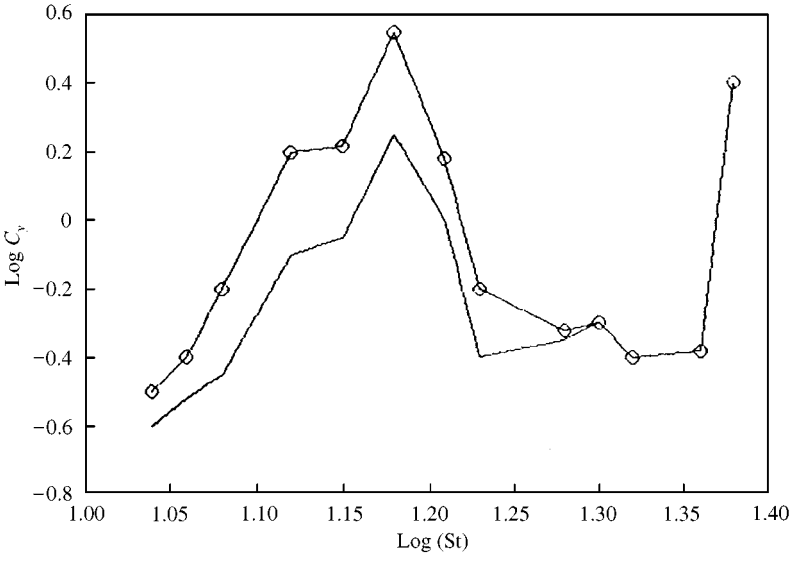

Figure 13. The combined effect of the perturbation amplitude and Strouhal number on the cavitating wing lift oscillations. The unmarked curve relates to $u = 0{\cdot}025$; those marked by O curve relates to $u = 0{\cdot}05$.

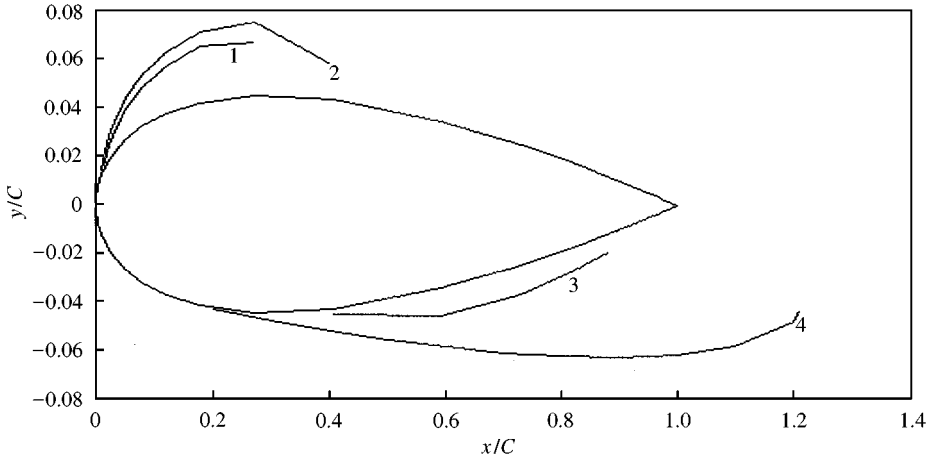

Figure 14. The effect of cavity detachment location on the cavity shape for the NACA-0009 hydrofoil. The cavities over the top and bottom parts of the hydrofoil correspond to the different flows. The top part shows cavities in viscous fluid (curve 1) and ideal fluid (curve 2) for $\sigma = 1{\cdot}5$ at $\alpha = 5°$. The bottom part shows cavities in viscous fluid (curve 3) and ideal fluid (curve 4) for $\sigma = 0{\cdot}15$ at $\alpha = 0°$. These cavities are plotted jointly for ease of comparison of these effects for small and high angles of attack.

The third discrepancy is associated with the scale effect on the cavity detachment location. This is not an appropriate place to describe the viscous–inviscid interaction theory that can forecast this location [see Amromin (1985) for its description]; however, it is appropriate to show certain results of such computations. One can see the consequence of the above effect in Figure 14, where results for an ideal fluid can be considered as an extreme case that corresponds to the very large scales. The scale effect on cavity length and volume is

especially high for low values of the wing angle of attack, and such low values are customary for marine propeller sections. This scale effect must amplify the contribution of subharmonics.

The fourth discrepancy is associated with the μ effect. Because of the higher values of U, the full-scale wings or blades are effectively softer, so their response to excitation should be smaller, and so should be the subharmonics.

An example of the qualitative comparison of the amplitudes of cavity volume oscillation is given in Figure 15, where numerical results are shown in which the four above-mentioned discrepancies have been taken into account. Scale effects on cavity detachment and length can be estimated in the framework of potential flow theory by variations in the X_1 and X_2 values for the same σ. These variations were found here with the use of the above-mentioned viscous–inviscid interaction theory. The scale effect on the excitation magnitude was estimated using typical empirical data (Amromin *et al.* 1993). Of course, such results are far from a direct prediction of the properties of the actual marine propellers. Rather they are a basis for a future examination. The auxiliary comparison of the second harmonic in Figure 16 may be even more useful as a basis for the qualitative analysis. The point is that experts offer two opinions: (a) that the dimensionless pressure pulsation is higher using model marine propellers; (b) that the higher pulsation corresponds to the full-scale subharmonics. The curves in Figure 16 have shown that the two opinions are not contradictory; the relatively high full-scale subharmonics can occur, but only in narrow intervals of the excitation that correspond to the significant Strouhal numbers.

6. CONCLUSIONS

The numerical simulation of the cavitating elastic wing vibration was made for various free-stream speeds, moduli of elasticity, fluid densities and wing densities. It was shown that the cavitation effects on wing vibration are more significant in the low-frequency bands, where the cavities multiply the number of the lift maxima and minima. The mono-frequency perturbation of the incoming flow causes the subharmonics of the wing response, as a result

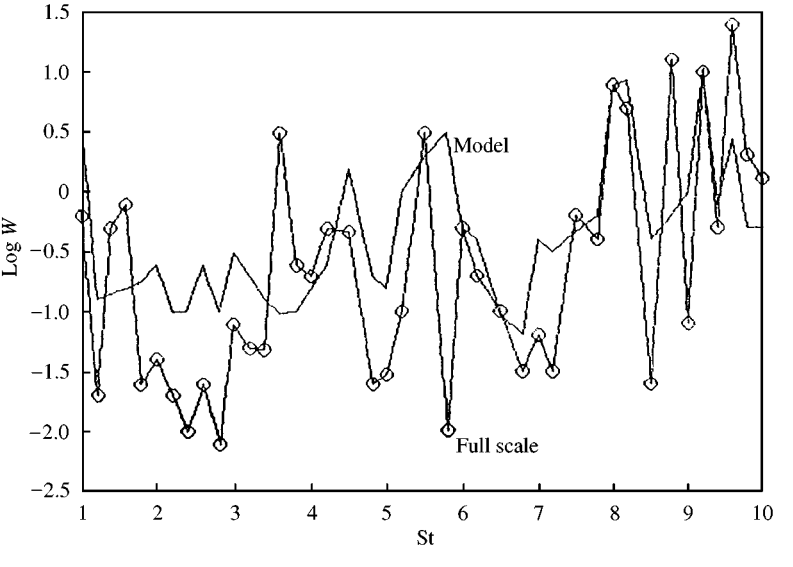

Figure 15. Comparison of amplitudes of the cavity volume oscillations for the model and full-scale conditions.

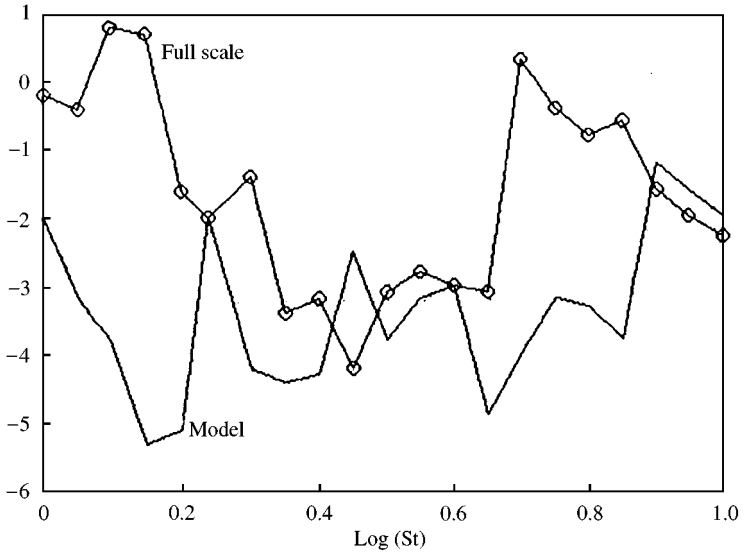

Figure 16. Comparison of the logarithm of the second harmonics of the cavity volume oscillation for the model and full-scale conditions.

of the parametric excitation of this wing by the oscillating cavity. The cavity volume oscillation is a nonlinear function of the incoming flow perturbation amplitude, so lift oscillation and the vibration level are nonlinear functions of this amplitude too. The most significant response of the cavitating elastic wing appears in the narrow intervals of the relatively low Strouhal number which is based on the time-averaged cavity length. This high response is associated with the high contribution of the subharmonics.

References

Amromin, E. L. 1985 On cavitation flow calculation for viscous capillary fluid. *Fluid Dynamics* **20,** 891–899.

Amromin, E. L., Briancon-Marjollet, L. & Vasiliev, A. V. 1994. Sheet cavitation: comparison between measured and computed length. *Proceedings International Shipbuilding Conference*, St-Petersburg, Vol. B, pp. 59–66.

Amromin, E. L., Vaciliev, A. V. 1994 Determination of the lift of a partially cavitating wing, *Fluid Dynamics* **29,** 797–799

Amromin, E. L., Vaciliev, A. V., Orlov, O. P. & Syrkin, E. N. 1993 Calculation of cavitation inception number for propellers including a method for wake effect. In *Cavitation Inception* (eds W. B. Morgan & M. Billet), ASME Vol. 177, pp. 103–112. New York: ASME.

Archibald, F. S. 1975 Unsteady Kutta condition at high value of the reduced frequency parameter, *Journal of Aircraft* **12,** 545–550

Blake, W. K. 1986 *Mechanics of Flow-Induced Sound and Vibration.* New York: Academic Press.

Boulon, O. & Chahine, G. L. 1998 Numerical simulation of unsteady cavitation on a 3-D wing. *Third International Symposium on Cavitation*, Grenoble, Vol. 2, pp. 249–256.

Dang, J. & Kuiper, G. 1998 Re-entrant Jet modeling of partial cavity flow on two dimensional wing, *Third International Symposium on Cavitation*, Grenoble, Vol. 2, 233–242.

Dowell, E. H., Crowley, E. F., Curtiss, H. C. Jr, Peter, D. A., Scanlan, R. H. & Sisto, 1978 *A Modern Course in Aeroelasticity*, 3rd edition. Dordrecht: Kluwer Academic.

Franc, J. P., Avellan, F., Belhadji, B., Billard, J. Y., Briançon-Mar, L., Frechou, D., Frouman, D. H., Karimi, A., Kveny, J. L. & Michel, J. M., 1995 *La cavitation.* Presses Universitaires de Grenoble (in French).

Gahkov, F. D. 1966 *Boundary Value Problems*. Oxford: Pergamon Press.
Kawanami, Y., Kato, H. & Yamaguchi, H. 1998 Three-dimensional characteristics of the cavities formed on a two-dimensional wings. *Third International Symposium on Cavitation*, Grenoble, Vol. 1, pp. 191–196
Kovinskaya, S. I & Amromin, E. L. 1997 Parametric vibration of elastic cavitating wing in unsteady flow. ASME Vol. AD **53–3**, pp. 121–128.
Kovinskaya, S. I. & Amromin, E. L. 1998 Oscillating partial cavity on elastic wing, *Third International Symposium on Cavitation*, Grenoble, Vol. 1, pp. 233–238.
Pellone, C. & Rowe, A. 1988 Effect of separation of partial cavitation. *ASME Journal of Fluids Engineering* **110,** 212–221.
Rashad, S. W. & Green, T. III, 1990 Steady performance of a flexible wing near a free surface, *Journal of Ship Research* **34,** 302–310.
Rowe, A. & Blottiaux, O. 1993 Aspects of modeling partially cavitating flows. *Journal of Ship Research* **37,** 39–50
Shin, B. A. & Ikohagi, T. 1998 A numerical study of unsteady cavitating flow. *Third International Symposium on Cavitation*, Grenoble, Vol. 2, pp. 301–306.
Yamaguchi, H. & Kato, H. 1993 Development of foil section with improved cavitation performance. *Journal of Society of Naval Architects of Japan* **154,** 95–101 (in Japanese).